# A Topological Test for Embeddings

C. Letellier*, I. M. Moroz†, & R. Gilmore*‡

* *Université de Rouen — CORIA UMR 6614, BP 12, F-76801 Saint-Etienne du Rouvray cedex, France*

†*Mathematical Institute, 24-29 St Giles', Oxford OX1 3LB, UK*

‡*Physics Department, Drexel University, Philadelphia, Pennsylvania 19104, USA*

(Dated: August 3, 2007, work in progress)

A new test for embedding time series data from low-dimensional chaotic systems into three-dimensional phase spaces is proposed. It is topological, based on the overcompleteness of the topological invariants of periodic orbits embedded in chaotic attractors. As such it is independent of artificial thresholds that accompany all other embedding tests. The test is illustrated on vector and scalar time series generated by a four-dimensional dynamical system.

A large number of experiments have been carried out on physical systems that exhibit chaotic behavior over some range of parameter values. In most cases a single observable is measured at equally spaced time intervals, resulting in a scalar time series $m_i = m(t_i)$, $i = 1, 2, \ldots, N$. Usually the first step in the analysis of such data is a search for a suitable embedding. An embedding is a mapping of the data into a phase space $R^D$ that preserves determinism, so that the original dynamical behavior can be reconstructed. If the data are chaotic, $D \geq 3$ [1].

Mappings of scalar time series into $R^D$ take the form $m(t) \to (x_1(t), x_2(t), x_3(t), \ldots, x_D(t))$, where the coordinates $x_i(t)$ are functions of the observables. A number of mappings have been proposed. The default is the time delay mapping, in which $x_i(t) = m(t - (i-1)\tau)$, where $\tau$ is the time delay [2–4]. Another very useful mapping is the differential mapping, in which $x_i(t) = d^{(i-1)}m(t)/dt^{(i-1)}$ [5]. Other useful mappings take the form of mixtures of these two types, for example $m(t) \to (m(t), dm(t)/dt, m(t-\tau))$, SVD mappings, and Hilbert transform pairs. Classes of mappings have been reviewed in [6–10].

Once observed data have been mapped into a $D$-dimensional phase space it is necessary to determine whether the mapping is an embedding. An embedding is a mapping that preserves determinism. That is, the mapped attractor avoids self-intersections, so that the uniqueness theorem is preserved. A number of embedding tests have been proposed. They all share a common feature: they are implemented as a function of increasing dimension and a mapping is declared an embedding when a threshold is reached. The tests are of *two* broad types: geometric and dynamical. Each type has many variants. The earliest test was geometric. It depended on computing geometric invariants [11] such as fractal dimensions and looking for "saturation of fractal dimensions" as a function of increasing dimension [12–14]. In practice this test was difficult to implement and is still more of a black art than science. This was superceded in practice by the "false nearest neighbor" test [15]. This test looks at two points near each other in some mapping and determines whether they remain near each other as the dimension increases. If 'yes', the two points are assumed near each other in the original attractor that generated the data. If 'no', the initial mapping did not provide an embedding. A mapping is declared an embedding when a sufficiently small percentage of point pairs are determined to be false nearest neighbors. Dynamical tests are similar in spirit. If a mapping is an embedding, then a point in $R^D$ has a unique future. Predictability of the future from the present was implemented in the "bad prediction" test [16]. This same property was implemented in another way as a "test for determinism" [17]. In this test the phase space was decimated in each dimension and the uniqueness of the flow direction in each $D$-dimensional cube was estimated by computing inner products of tangent vectors to all trajectories passing through each cube. Both these dynamical tests declare a mapping to be an embedding when the relevant statistic reaches an appropriate value.

Behind all these tests lurk the embedding theorems. These guarantee that if the dynamics is generated by an $n$-dimensional dynamical system, the data describing the dynamics can always be embedded in $R^D$ for $D$ sufficiently large. These theorems are based on the idea that if the dimension is sufficiently large there is enough room in phase space so that self-intersections typically ("generically") do not occur. The simplest estimate $D \geq 2n+1$ based on genericity was reduced to $D \geq 2n$ by Whitney [18] and reduced once again to $D > 2d_A$ [19], where $d_A$ is an appropriate fractal dimension. For the Lorenz attractor [21] with $d_A = 2.06$ these theorems guarantee that an embedding into $R^D$ with $D \geq 5$ can always be found. As pointed out forcefully by Abarbanel and collaborators [6, 7, 15], pleasing as it might be to mathematicians to have a theorem of this type, for physicists such theorems are useless. If the dynamics is three-dimensional we

need an algorithm for constructing a three-dimensional embedding rather than a theorem stating that a five-dimensional embedding exists.

Once a suitable embedding has been determined, the embedded data can be analyzed. The analysis procedures are of *three* broad types: geometric [13], dynamical [20], and topological [5]. Geometrical and dynamical analyses focus on computing the spectra of fractal dimensions and Lyapunov exponents, respectively. These calculations can be carried out for any value of the dimension $D$. The results are real numbers with no underlying statistical theory to provide believable error estimates (error bars are "educated guesses" [14]), and no information about the mechanism that generates chaotic behavior. Topological analyses can be carried out only when $D = 3$. However, these tests reveal the mechanism that generates chaotic behavior. Furthermore, the results are overdetermined and therefore contain their own rejection criteria [5, 9]. We will exploit this overdeterminism and rejection criteria in this new test for embedding in $R^3$. The restriction to three dimensions is not as problematic as it might seem. All of the embedding tests described above were benchmarked primarily on low-dimensional flows generated by the standard chaotic attractors such as the Lorenz [21] and Rössler [45] attractors. Further, our understanding of the description and properties of three-dimensional attractors (those that exist in a three-dimensional phase space) far exceeds our understanding of higher-dimensional attractors. For these reasons the present topological test for embedding in three dimensions presents a powerful complement to embedding tests based on geometry and dynamics. A comparison of the geometrical, dynamical, and topological tools and their application to tests of embeddings and analyses of chaotic data is presented in Table I.

TABLE I: Relation among the geometrical (G), dynamical (D), and topological (T) methods of analyzing and embedding chaotic data. Dim. is the dimension for which the test is applicable; Rej. indicates whether the test contains its own rejection criteria.

| | Embedding | Dim. | Rej. | Analysis | Dim. | Rej. |
|---|---|---|---|---|---|---|
| G | Correlation dim. | $\geq 3$ | N | Fractal dims. | $\geq 3$ | N |
| | False NN | | | Lyapunov dim. | | |
| D | Bad prediction | $\geq 3$ | N | Lyapunov exps. | $\geq 3$ | N |
| | Determinism | | | | | |
| T | Linking #s | 3 | Y | Linking #s | 3 | Y |

The basic idea of and algorithm for this test is simple to state. Estimate the Lyapunov dimension, $d_L$, from $m(t)$ [22]. If $d_L > 3$, stop. Otherwise follow these steps: (1) Search through the scalar time series $m(t)$ for surrogates for periodic orbits. This can be done by the method of close returns before any embedding is attempted [25, 26]. (2) Choose a mapping and (3) construct a generating partition for this mapping [27]. (4) Construct a table of linking numbers for the periodic orbits identified in step (1) [28]. (5) Construct the branched manifold based on a small number of lower-period orbits [29] and (6) compare the predicted and computed linking numbers for the rest of the orbits identified in the data. If there is any disagreement then (a) the mapping is not an embedding; or (b) the symbolic labeling of one or more orbits is questionable; or (c) the branched manifold is incorrect. This algorithm can be repeated over many mappings until a suitable embedding is found, if ever. Items (b) and (c) are part of the analysis procedure; item (a) is the heart of this new embedding test.

We illustrate this algorithm using data generated by the four-dimensional dynamical system:

$$\begin{aligned} \dot{X} &= \sigma(-X + Y) - 7.1111\beta U \\ \dot{Y} &= (R/\nu)X - Y - XZ \\ \dot{Z} &= -\nu Z + XY \\ \dot{U} &= -\Lambda U + X \end{aligned} \tag{1}$$

This system is a modification of the Malkus-Robbins dynamo equations (involving only $(X, Y, Z)$) which were originally introduced to model the action of a self-exciting dynamo. The extension is to include the variable $U$, which represents the angular speed of the motor of the dynamo [38]. For $\beta = 0$ there is no feedback from the $U$ subsystem into the $(X, Y, Z)$ subsystem, which behaves like a Lorenz attractor. The four-dimensional system is *reducible* in this case [9]. The dynamics was studied for $(\sigma, \nu, R) = (10, 8/3, 74.667)$, where the Lorenz equations generate a chaotic attractor, and $\Lambda = 3.2$. In the range $0 \leq \beta < 7.9$, Eq. (1) generates a chaotic attractor with Lyapunov dimension $D_L \simeq 2.2$ [48]. A boundary crisis destroys the attractor at $\beta \simeq 7.9$.

Surrogate periodic orbits were extracted from the chaotic time series by the method of close returns [24, 25]. These were extracted using the full $(X(t), Y(t), Z(t), U(t))$ time series and the scalar time series $Y(t)$ alone. A symbolic dynamics on two symbols $L$ and $R$ was constructed using a projection into the $Y$-$\dot{Y}$ plane, shown for $\beta = 3.8$ in Fig. 1. Projections for other values of $\beta$, and projections into other subspaces (except $(Z, \dot{Z})$) looked similar. The topological entropy of this system is slightly less than $\log 2$ so most orbits on two symbols were present. The two exceptions were the two period-one orbits $L$ and $R$.

Each mapping into $R^3$ was tested as an embedding as follows. The orbits were mapped into $R^3$ and a table of linking numbers was constructed. The mapping was considered an embedding if this table was consistent with a table of linking numbers that could be constructed for this spectrum of orbits using some branched manifold.

The first mapping we tested was the projection $R^4 \to R^3$ given by $(X, Y, Z, U) \to (X, Y, Z)$. For $0.6 < \beta < 5.4$ the table of linking numbers obtained from the unstable periodic orbits was not compatible with any branched manifold. For $0 \leq \beta < 0.6$ and $5.4 < \beta < 7.9$ the tables were compatible with linking numbers derived

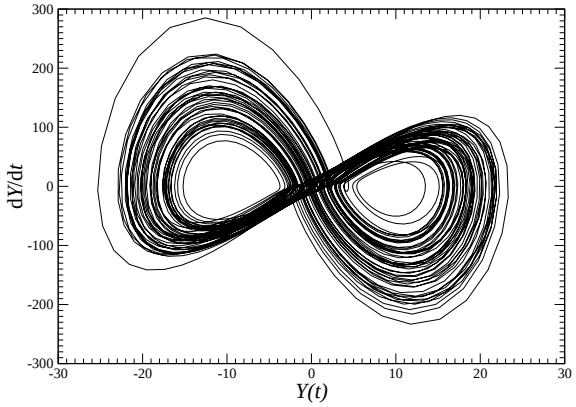


FIG. 1: Projection of the chaotic attractor onto the two-dimensional subspace $(Y, \dot{Y})$ provides coding information. Parameter values: $(\sigma, \nu, R, \Lambda) = (10, 8/3, 74.667, 3.2)$ and $\beta = 3.8$.

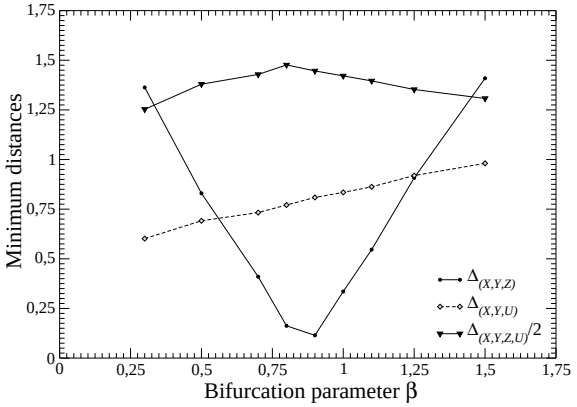


FIG. 2: Minimum distance between the two surrogate orbits $LRR$ and $LLR$ as a function of $\beta$ in the chaotic attractor in $R^4$ and under two projections into three-dimensional spaces. Under the mapping $(X, Y, Z, U) \to (X, Y, Z)$ these orbits undergo an intersection: this mapping cannot be an embedding for all values of $\beta$. Parameter values: $(\sigma, \nu, R, \Lambda) = (10, 8/3, 74.667, 3.2)$.

from Lorenz branched manifolds with rotation symmetry [30, 31, 33, 44]. Moreover, we found that for each pair of orbits $A$ and $B$, the linking number $LN(A, B)$ in the large $\beta$ limit was the *negative* of its value in the small $\beta$ limit. This means that the branched manifold in the large $\beta$ limit is the mirror image of the branched manifold in the small $\beta$ limit [48]. This comes about because the mapped attractor undergoes self-intersections, inverting itself in the process as $\beta$ increases.

When self-intersections occur, pairs of periodic orbits "pass through" each other. A robust way to determine when this occurs is to locate two periodic orbits whose linking number ($LN$) changes from a value compatible with the Lorenz template to a value incompatible with any branched manifold somewhere in the range $0.6 < \beta < 5.4$. This test was carried out on two period-three orbits, $LLR$ and $RRL$. For these orbits, $LN(LLR, RRL) = +1$ for $0 \le \beta < 0.85$, 0 for $0.85 < \beta < 4.0$ and and $-1$ for $5.0 \le \beta < 7.9$.

To show these orbits intersect, we computed the minimum distance between them as a function of $\beta$ in three different spaces: the four-dimensional space with coordinates $(X, Y, Z, U)$ and the two three-dimensional projections $(X, Y, Z)$ and $(X, Y, U)$. The result is presented in Fig. 2, which clearly shows that $LLR$ and $RRL$ intersect between $\beta = 0.85$ and $\beta = 0.9$ only in the $(X, Y, Z)$ projection. The region of self-intersection of the attractor begins at smaller values of $\beta$, as can be seen by analyzing the linking numbers of higher period orbits. The minimum distance between these two orbits in $R^4$ is never zero by genericity arguments.

The differential mapping based on $Y(t)$ into three dimensions was also investigated. The linking numbers for the appropriate branched manifold, the Lorenz branched manifold with inversion symmetry, are given in Table II. Analysis of the linking numbers revealed that this was not an embedding for values of $\beta$ in the range

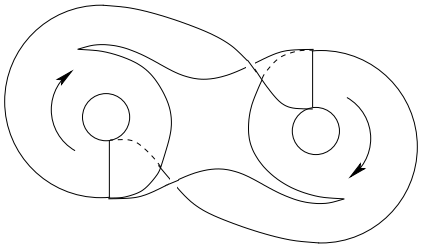

FIG. 3: Lorenz branched manifold with inversion symmetry. This describes the topological organization of all the unstable periodic orbits for embeddings obtained by projections into $(X, Y, U)$ and differential embeddings based on the odd variables $X(t)$ and $U(t)$.

$0.6 < \beta < 5.4$. This zero-parameter family of mappings was replaced by the one-parameter family of delay mappings $(Y(t), Y(t-\tau), Y(t-2\tau))$. In the limit of small $\tau$, this is equivalent to the differential mapping. We studied this mapping as a function of $\tau$ for data generated at $\beta = 3.8$. For small $\tau$ the linking numbers did not agree with those compatible with any branched manifold. As $\tau$ is increased, the linking numbers that were incompatible with the branched manifold shown in Fig. 3 changed because of intersections until all reached values compatible with this branched manifold for a small range of delay values above $\tau = 10$. In Fig. 4 we show the minimum distance between orbits $LRR$ and $LLRR$ as a function of $\tau$. An intersection occurs near the delay $\tau \simeq 10$. For $\tau = 7$ $LN(LRR, LLRR) = 0$ and for $\tau = 13$ $LN(LRR, LLRR) = -1$: the former incompatible and the latter compatible with the branched manifold in Fig. 3 and Table II. the linking number changes at other orbit intersections.

TABLE II: Linking numbers of low period orbits in the inversion-symmetric Lorenz attractor.

| | $LR$ | $LLR$ | $LRR$ | $LLLR$ | $LRRR$ | $LLRR$ |
|---|---|---|---|---|---|---|
| $LR$ | $-$ | 0 | 0 | 0 | 0 | 0 |
| $LLR$ | 0 | $-$ | 0 | $+1$ | 0 | $+1$ |
| $LRR$ | 0 | 0 | $-$ | 0 | $-1$ | $-1$ |
| $LLLR$ | 0 | $+1$ | 0 | $-$ | 0 | $+1$ |
| $LRRR$ | 0 | 0 | $-1$ | 0 | $-$ | $-1$ |
| $LLRR$ | 0 | $+1$ | $-1$ | $+1$ | $-1$ | $-$ |

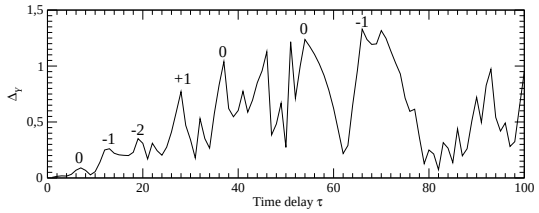


FIG. 4: Minimum distance between orbits $LRR$ and $LLRR$ in the time delay mapping $(Y(t), Y(t-\tau), Y(t-2\tau))$ as a function of the time delay $\tau$. The integers above some peaks is $LN(LRR, LLRR)$. The characteristic period corresponds to $\tau \simeq 80$.

Fig. 5 shows a simple "cardboard model" representation of the geometric structure created by the projection $(X, Y, Z, U) \to (X, Y, Z)$ for $\beta = 3.8$ when it is not an embedding. The dark line indicates the region in the $(X, Y, Z)$ phase space where the two lobes of the attractor undergo self-intersections. This set of dimension $2 \times 2.2 - 3 \simeq 1.4$ [34] has measure zero, and is the region responsible for failure to embed. Most of the geometrical tests and all of the dynamical tests for embedding depend upon picking up a signal from this measure zero set. This small signal could easily be obscured by choice of threshold parameters for these two classes of tests. On the other hand there is no way to misinterpret the zero-crossing signatures in Figs. 2 and 4.

In order to complete the symmetry that exists between methods for analyzing chaotic data and methods for testing whether a mapping is an embedding or not, in this Letter we have introduced a new embedding test. This test depends upon the rigid organization of the unstable periodic orbits that exist in abundance in three-dimensional chaotic attractors, and the description of this organization by branched manifolds. More specifically, for a mapping to be an embedding, it must preserve the results of the Birman-Williams theorem for low-dimensional chaotic attractors [35]. The three analysis techniques and the symmetry between embedding tests and analyses once an embedding has been found are summarized in Table I.

R. G. thanks CNRS for the invited position at CORIA for 2006-2007.

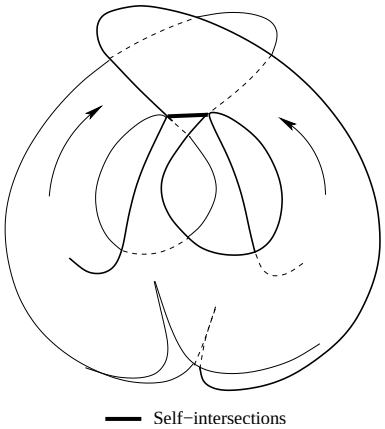


FIG. 5: Cardboard model of the self-intersections of the projection of the chaotic attractor into the $(X, Y, Z)$ subspace for $0.6 < \beta < 5.4$.

## REFERENCES


[1] E. Ott, Revs. Mod. Phys. **53**, 655 (1981).

[2] F. Takens, in: *Proceedings of the Symposium on Dynamical Systems and Turbulence, Warwick, 1979-1980*, (D. Rand and L. S. Young, eds.) Lecture Notes in Mathematics **898**, Berlin: Springer-Verlag, 1981, p. 366.

[3] R. Mañé, in: *Proceedings of the Symposium on Dynamical Systems and Turbulence, Warwick, 1979-1980*, (D. Rand and L. S. Young, eds.) Lecture Notes in Mathematics **898**, Berlin: Springer-Verlag, 1981, p. 230.

[4] N. H. Packard, J. P. Crutchfield, J. D. Farmer and R. S. Shaw, Geometry from a time series, Phys. Rev. Lett. **45**, 712 (1980).

[5] G. B. Mindlin, H. G. Solari, M. A. Natiello, X.-J. Hou, and R. Gilmore, J. Nonlinear Sci. **1**, 147 (1991).

[6] H. D. I. Abarbanel, R. Brown, J. J. Sidorowich, and L. Tsimring, Revs. Mod. Phys. **65**, 1331 (1993).

[7] H. D. I. Abarbanel, *Analysis of Observed Chaotic Data*, New York: Springer, 1996.

[8] H. Kantz and T. Schreiber, *Nonlinear Time Series Analysis*, Cambridge: Cambridge University Press, 1997.

[9] R. Gilmore, Topological analysis of chaotic dynamical systems, Rev. Mod. Phys. **70**, 1455 (1998)

[10] R. Gilmore and M. Lefranc, *The Topology of Chaos*, NY: John Wiley & Sons, 2002.

[11] P. Grassberger, Phys. Lett. A**97**, 227 (1983).

[12] P. Grassberger and I. Procaccia, Estimation of the Kolmogorov entropy from a chaotic signal, Phys. Rev. A**28**, 2591 (1983).

[13] P. Grassberger and I. Procaccia, Measuring the strangeness of strange attractors, Phys. Lett. D**148**, 63 (1983).

[14] P. Grassberger and I. Procaccia, Characterization of strange attractors, Phys. Rev. Lett. **50**, 346 (1983).

[15] M. B. Kennel, R. Brown, and H. D. I. Abarbanel, Determining embedding dimension for phase space reconstruction using a geometrical construction, Phys. Rev. A**45**, 3403 (1992).
[16] G. Sugihara and R. M. May, Nature (London) **344**, 734 (1990).
[17] D. T. Kaplan and L. Glass, Phys. Rev. Lett. **68**, 427 (1992).
[18] H. Whitney, Differentiable manifolds, Ann. Math. **37**, 645 (1936)
[19] T. Sauer, M. Casdagli, and J. A. Yorke, Embeddology, (1991).
[20] A. Wolf, J. B. Swift, H. L. Swinney, and J. A. Vastano, Physica (Amsterdam) 16**D**, 285 (1985).
[21] E. N. Lorenz, Deterministic nonperiodic flow, J. Atm. Sci. **20**, 130 (1963)
[22] J. L. Kaplan and J. A. Yorke, in *Functional Differential Equations and Approximations of Fixed Points*, (JH. O. Peitgben and H. O. Walther, eds), Springer Lecture Notes in Mathematics, New York: Springer-Verlag, 1979.
[23] O. E. Rossler "close returns" somewhere, (1975?)
[24] J.-P. Eckmann, S. O. Kamphorst, and D. Ruelle, Recurrence plots of dynamical systems, Europhys. Lett. **5**, 973 (1987)
[25] D. Auerbach, P. Cvitanovic, J.-P. Eckmann, G. Gunaratne, and I. Procaccia, Phys. Rev. Lett. **58**, 2387 (1987).
[26] D. Lathrop and E. J. Kostelich, Phys. Rev. A**40**, 4028 (1989).
[27] P. Grassberger and H. Kantz, Genereating partitions for the dissipative Henon map, Phys. Lett. A**113**, 235 (1985).
[28] H. G. Solari and R. Gilmore, Relative rotation rates for driven dynamical systems, Phys. Rev. A**37**, 3097 (1988).
[29] G. B. Mindlin, X.-J. Hou, H. G. Solari, R. Gilmore, and N. B. Tufillaro, Phys. Rev. Lett. **64**, 2350, (1990).
[30] C. Letellier & R. Gilmore. Covering dynamical systems: Two-fold covers, *Physical Review E*, **63**, 16206, 2001.
[31] R. Gilmore and C. Letellier, Phys. Rev. E (2003).
[32] G. Byrne, R. Gilmore & C. Letellier, Distinguishing between folding and tearing mechanisms in strange attractors, *Physical Review E*, **70**, 056214, 2004.
[33] R. Gilmore and C. Letellier, *The Symmetry of Chaos*, NY: Oxford University Press, 2006.
[34] R. Gilmore, *Catastrophe Theory for Scientists and Engineers*, NY: Wiley, 1981.
[35] J. Birman and R. F. Williams, Topology **20**, 1 (1983). **Check this.**
[36] R. Hide, A. C. Skeldon, & D. J. Acheson, D, A study of two novel self-exciting single-disk homopolar dynamos: theory, *Proc. R. Soc. Lond.* A **452**, 1369–1395 (1996).
[37] R. Hide, & I. M. Moroz, Effects due to induced azimuthal eddy currents in the self-exciting Faraday disk homopolar dynamo with a nonlinear series motor: I Two special cases, *Physica D* **134** 287–301 (1999).
[38] I. M. Moroz, The Malkus-Robbins dynamo with a linear series motor, *Int. J. Bifurcation and Chaos* **13**, 147–161 (2003).
[39] I. M. Moroz, The extended Malkus-Robbins dynamo as a perturbed Lorenz system, *Nonlinear Dynamics* **41**, 191–210 (2005).
[40] K.A. Robbins, A new approach to sub-critical instability and turbulent transitions in a simple dynamo, Math. Proc. Cambridge Philos. Soc., **82**, 309-325 (1977).
[41] I. Moroz, The Malkus-Robbins dynamo with a linear series motor, *International Journal of Bifurcations & Chaos*, **13**, 147-161, 2004.
[42] C. Letellier & L. A. Aguirre, Investigating nonlinear dynamics from time series: the influence of symmetries and the choice of observables, *Chaos*, **12**, 549-558, 2002.
[43] C. Letellier & L. A. Aguirre, Graphical interpretation of observability in terms of feedback circuits, *Physical Review E*, **72**, 056202, 2005.
[44] I. Moroz, C. Letellier, and R. Gilmore, (unpublished).
[45] O. E. Rössler, An equation for continuous chaos, Phys. Lett. A**57**, 397 (1976).
[46] J. Milnor and W. Thurston, *Dynamical Systems*, (J. C. Alexander, ed.) Lecture Notes in Mathematics No. **1342**, New York: Springer, 1987.
[47] J.-P. Eckmann and D. Ruelle, Ergodic theory of chaos and strange attractors, Rev. Mod. Phys. **57**, 617 (1985).
[48] I. M. Moroz, C. Letellier, and R. Gilmore, (unpublished).